13th World Conference on Earthquake Engineering
Vancouver, B.C., Canada
August 1-6, 2004
Paper No. 1464

SEISMIC PERFORMANCE OF OLDER BEAM-COLUMN JOINTS

Dawn LEHMAN[1], John STANTON[2],
Meredith ANDERSON[3], Daniel ALIRE[4], Steve WALKER[5]

SUMMARY

Performance evaluation of a non-ductile reinforced concrete frame requires reliable estimates of the engineering response, including strength, stiffness, and damage states. Typically, the components that contribute to the response include beams, column, and joints. Although a significant number of studies have addressed the response of older beams and columns, few have evaluated the response of older beam-column joints. These older joints typically have no transverse reinforcement but in some cases may be subjected to high joint shear stress demands. The influence of the joint deformations on the response can be significant, but, in engineering practice, the joints are typically modeled as rigid elements and the effects of their deformations are neglected.

A research program was conducted to develop tools for the performance evaluation of joints in older reinforced concrete frame construction. Initially, eleven experimental specimens were tested. The specimens were designed to study joint behavior over a range of material strengths and joint shear stress demands. In addition, the influence of displacement history was investigated using nominally identical specimens. The results were used to quantify important response parameters including stiffness, strength, and damage. The measured response formed the basis of an advanced constitutive model for the joint shear-stress strain response. The model uses a tri-linear backbone curve with nonlinear branch curves and includes pinching in the response. In the experiments, degradation was noted in the stiffness, strength and pinching, specifically in cycles that exceeded a threshold strain. In the model, degradation relationships were developed to simulate this response. Mathematically, these relationships depend on the ratio of the current strain demand to the previous maximum strain (in the case of stiffness) or to the threshold strain (in the case of strength and pinching). The predicted response using the resulting model compared well with the measured response in both these experiments and those from and an independent set conducted by others.

[1] Assistant Professor, University of Washington, Box 352700, Seattle WA 98195
[2] Professor, University of Washington, Box 352700, Seattle WA 98195
[3] Former Graduate Student, University of Washington, Box 352700, Seattle WA 98195
[4] Former Graduate Student, University of Washington, Box 352700, Seattle WA 98195
[5] Former Graduate Student, Box 352700, Seattle WA 98195

INTRODUCTION

Reinforced concrete frames constructed prior to the 1970s are susceptible to damage under seismic loading. Joints in these frames may be subjected to high shear stresses. In current seismic design, limits on joint shear stresses play a dominant role in determining the column size in reinforced concrete frames, but this was not always the case. Prior to the pioneering experiments of Hanson and Connor (1967), codes did not specify limits on the joint shear stress or require joint transverse reinforcement, and as a result older joints have a wide range of shear stresses and typically do not contain transverse reinforcement. The mid 1970s saw the adoption of prescriptive rules for seismic design that resemble closely those in force today. However buildings constructed before that time were not detailed using modern codes and therefore the robustness of their seismic performance is open to question.

Seismic evaluation of these frames requires accurate estimates of the frame response and damage, which in turn requires analytical models for the elements, including the beams, columns, and beam-column joints. Although previous research has focused on damage to columns, most studies have neglected the beam-column joints. The joint flexibility is important because it increases the drift demand, which may lead to more non-structural damage and to structural instability through P-delta effects. However, practicing engineers usually ignore joint shear deformations in their analyses and the results of those analyses may therefore not be reliable. Although joint models exist, most are capable of simulating joints that meet the current code provisions and are subjected to monotonically increasing imposed cyclic deformation histories. Those models have limited applicability to older joints and more random cyclic deformation demands due to limitations in the calibration and validation data.

To better understand and model the seismic performance of joints in older frame buildings, a coordinated experimental and analytical study of older beam-column joints was undertaken. The joints studied in the experimental research simulated pre-1970s construction in that they contained no transverse reinforcement and were subjected to a wide range of joint shear stress demands. Eleven specimens were constructed and tested (Walker 2001, Alire 2002) to investigate the nature of shear resistance in older joints. The results provided insight into the influence of joint shear stress demand and concrete strength on joint performance, formed the basis for damage models that relate joint damage to local engineering parameters such as shear stress and strain.

Equally important, the experimental data were used to develop and calibrate a constitutive model that was developed to represent the joint shear-stress strain response of joints in older construction. The model is capable of simulating the response of reinforced concrete joints without transverse reinforcement to a wide variety of input motions. Here, key aspects of the model, including its primary parameters and its calibration and validation, are presented.

EXPERIMENTAL EVALUATION OF JOINT PERFORMANCE

Prior to planning the test program, a limited survey was conducted of reinforced concrete frame buildings constructed before 1973, which was the first year in which the UBC (Uniform 1997) incorporated ductile detailing requirements. A wide range of beam and column proportions was found, and the joints hear stress demands varied from 0.03 to $0.37f'_c$. The primary deficiencies were: column bar splices that were too short and that were located directly above the floors, lack of transverse reinforcement in the joints, inadequate transverse steel in the beams and columns, inadequate anchorage of the bottom beam bars in the column, and column/beam flexural strength ratios that were too low. Furthermore, the beam centerlines were in several cases offset from those of the columns. The scope of the project prevented all of these deficiencies from being studied, so the specimens were designed to focus on the joint shear behavior.

Test Program

The test program consisted of eleven specimens. The specimens all had the same geometry, which is shown in Figure 1. The column bars were continuous, to eliminate the possibility of premature splice failure, and the beams and columns were detailed in accordance with the principles of capacity design, as embodied in ACI 318-02. The joints contained no transverse reinforcement, and the joint shear stress demand was varied by suitable selecting suitable beam bars.

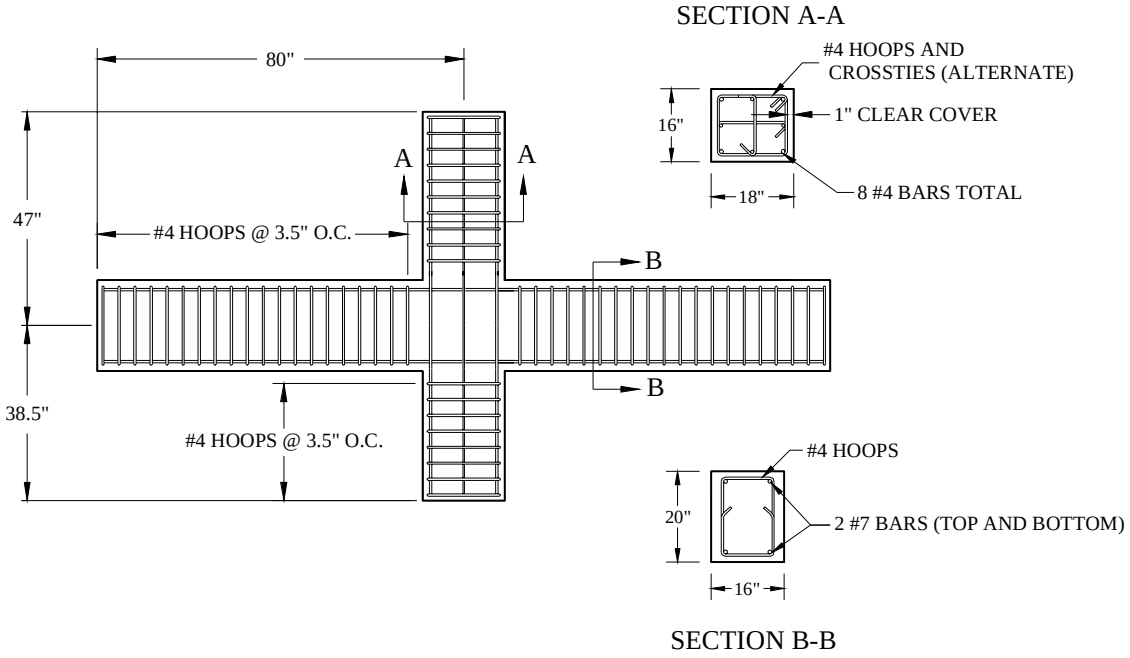

Figure 1 Test Specimen Dimensions (Reinforcement for PEER 0850 Shown)

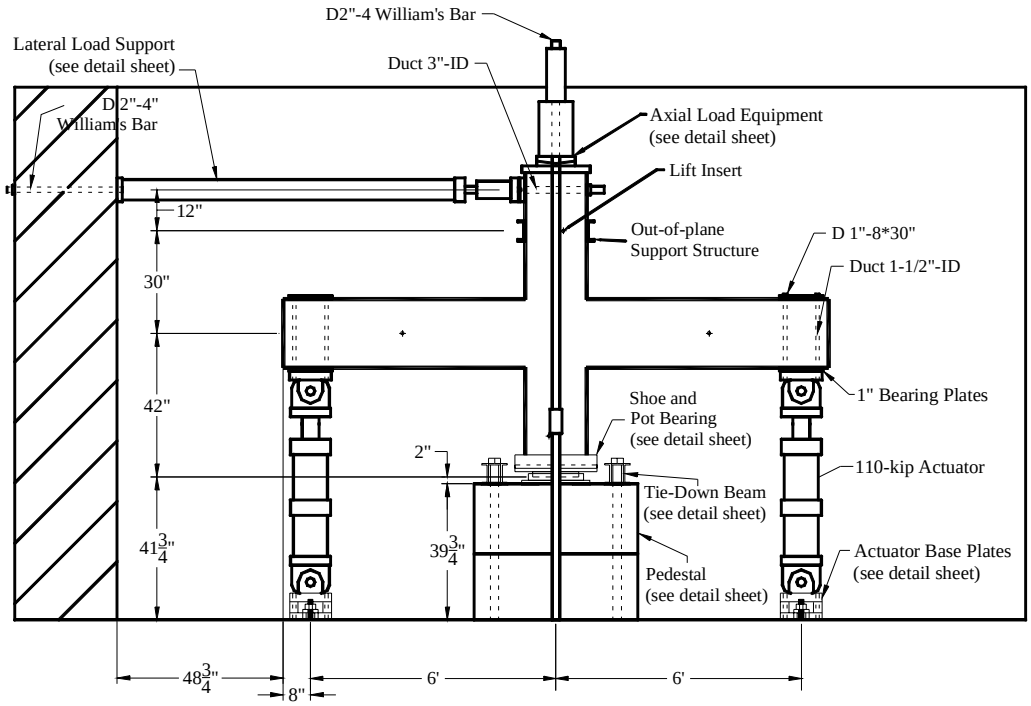

Figure 2 Test Setup

The specimens were set in a vertical plane for testing, as shown in Figure 2. Equal and opposite displacements were imposed at the beam ends by two servo-controlled actuators while the top and bottom of the column were fixed against translation and pinned against rotation. An axial load of $0.1f'_cA_g$ was applied to the column using a steel cross beam and high strength rods stressed to the strong floor. The principal instrumentation consisted of LVDTs at the beam tips, two joints shear strain rigs attached to threaded rods embedded in the joint concrete, and strain gages on the beam bars. Each joint shear strain rig consisted of six potentiometers, arranged in the sides and diagonals of a rectangle, from which the shear strain could be computed. The two rigs were attached on opposite faces of the column. The strain gages were attached, using a technique pioneered by Raynor (2000), in the bottom of slots milled along the bars. This method avoids the interruption to the bond that would otherwise be caused by the waterproofing over the gages when they are attached to the curved surface of the bar.

The test matrix is shown in Table 1, in which the test specimens are arranged in order of increasing amounts of normalized joint shear stress, $v_j/\sqrt{f'_c}$. The specimen naming system consists of the displacement history name (discussed below) followed by two digits that define the target shear stress demand as a fraction of f'_c, and two more digits that define f'_c. Thus, PEER 0850 has $v_{j,max} = 0.08f'_c$, and $f'_c = 5000$ psi.

Four displacement histories were used:

- **PEER**: sets of three equal cycles, with the amplitude of each set approximately 30% larger than the previous one. This was selected because such histories have been widely used in the past.
- **CD15:** 30 cycles with ***c***onstant ***d***isplacement amplitude of 1.5% drift ratio, followed by 12 cycles at 3%, then cycling at 5% drift ratio to failure. This was intended to simulate a distant, long-duration earthquake.
- **CD30:** 12 cycles with ***c***onstant ***d***isplacement amplitude of 3.0% drift ratio, followed by cycling at 5% drift ratio to failure.
- **PADH:** (***P***ulse ***A***symmetric ***D***isplacement ***H***istory). A highly asymmetric history starting with a half-cycle to 5% drift. This was intended to simulate the effects of a near-source, pulse-type earthquake.

Table 1 Test Matrix

Phase	Specimen	Target f'_c (psi)	Target v_j (psi)	Target v_j/f'_c	Target v_j/f'_c	History
II	PEER 0850	5000	400	0.08	5.7	PEER
II	PEER 0995	9500	855	0.09	8.5	PEER
I	PEER-1450	5000	700	0.14	9.1	PEER
I	CD15-1450	5000	700	0.14	9.1	CD15
I	CD30-1450	5000	700	0.14	9.1	CD30
I	PADH-1450	5000	700	0.14	9.1	PADH
II	PEER 1595	9500	1425	0.15	14.4	PEER
I	PEER-2250	5000	1100	0.22	14.8	PEER
I	CD30-2250	5000	1100	0.22	14.8	CD30
I	PADH-2250	5000	1100	0.22	14.8	PADH
II	PEER 4150	5000	2050	0.41	28.3	PEER

The work was conducted in two phases. In Phase I, consisting of seven specimens (Walker 2001), the primary variables were the target joint shear demand (9 or $15\sqrt{f'_c}$ psi) and the displacement history. In Phase II, (Alire 2002), four more specimens with different joint shear stress demands and two different

concrete strengths, were tested. The goal was to study the effects of joint shear stress, both in the absolute and as a proportion of the concrete strength. The PEER load history was used in all four cases.

Experimental Performance

The experimental data were used to assess the seismic performance of beam-column joints in non-ductile reinforced concrete frame construction. Four aspects of joint performance are of great interest. First, the compressive strength of the joint must be sufficient to carry the gravity load on the column. This condition was satisfied in every test, even when the joint damage was so severe that the center of the joint was destroyed and a hole existed right through it. This result is, in fact, predictable. If the concrete in the joint loses all of its axial strength, but is still able to support the bars against buckling, an axial load of $P = \alpha f'_c A_g$ can be supported by the bars alone, at a stress of f_y, if $\rho > \alpha f'_c / f_y$ where ρ is the column longitudinal reinforcement ratio. The minimum permissible reinforcement in a column is 1%, so a column with f'_c = 5000 psi can support a load of $0.12 f'_c A_g$ on the bars alone. More heavily reinforced columns can carry a proportionately higher load.

The second behavioral feature of interest is the shear strength of the joint. The traditional viewpoint is that the joint has a certain strength in shear, often taken to be 12, 15 or $20\sqrt{f'_c}$ (psi), depending on the arrangement of beams framing into it, as specified by ACI318-02 for joints containing transverse reinforcement. The experiments showed that, for joints without transverse reinforcement, this description is not valid, and that the strength varies significantly with bar yielding and displacement history. For example, joints in specimens PEER-0850 and PEER-4150 were essentially identical, but were subjected to target joint shear demands of $5.7\sqrt{f'_c}$ and $28.3\sqrt{f'_c}$ (psi) respectively. Yet both reached peak loads defined by their joint shear demands, and both suffered major damage to the joint region. If the joint shear strength was a unique value (in this case at least equal to $28.3\sqrt{f'_c}$ (psi)) then specimen PEER-0850 would have suffered no joint damage. Furthermore, the way in which failure progressed in the two specimens differed significantly. PEER-0850 underwent many cycles of beam yielding before suffering joint damage, while the beam bars in PEER-4150 had barely yielded when the joint failed in shear. This suggests that a joint shear stress demand of $5.7\sqrt{f'_c}$ (psi) represents approximately the value that separates pure beam yielding failure from joint shear failure, and that $28.3\sqrt{f'_c}$ (psi) is the joint shear demand above which beam yielding will not occur.

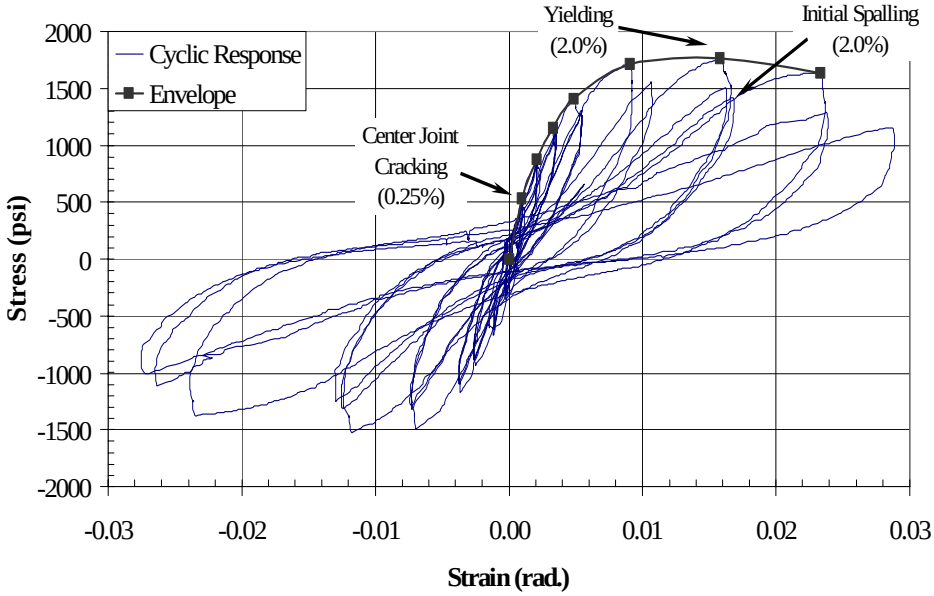

Figure 3. Joint Shear Stress vs. Strain for Specimen PEER 4150.

The third and fourth critical features of joint behavior are the joint stiffness and damage accumulation. They are related, because both change as the displacement history progresses. In the experiments, the stiffness of the beam and column changed little during the test, because they contained transverse reinforcement that complied with contemporary standards, but the joint stiffness dropped significantly as damage occurred. This can be seen in the joint shear stress vs. strain plots, such as the one for PEER 4150 shown in Figure 3. It can also be seen in a plot of the displacement components, such as shown in Figure 4 for Specimen PEER 1450. As can be seen, the joint deformation provided about 10% of the total at cycle 9 (to an applied drift ratio = 0.5%, which was the first cycle set after joint cracking) and, at the end of the test, it provided 75% of the total drift. This finding shows that modeling the joints in a frame analysis as rigid is likely to lead to a significant underestimate of the lateral drift. The drift affects not only the damage to the non-structural components, but also the possibility of instability due to P-Δ effects.

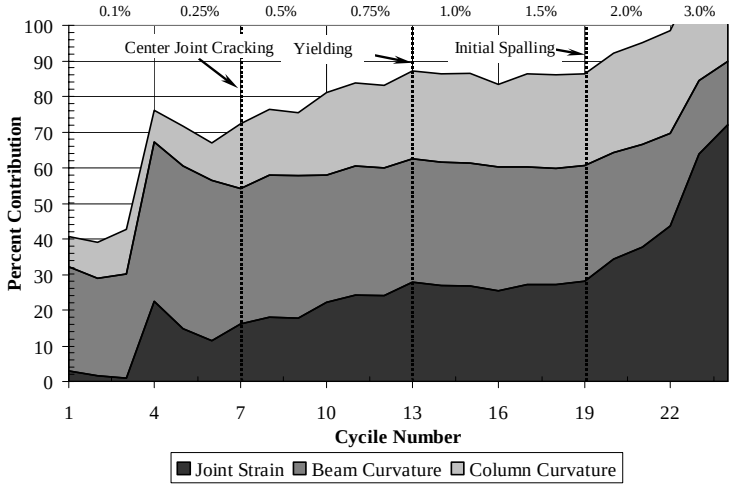

Figure 4 Components of Drift (Specimen PEER 0995)

The damage states identified were:

- Center joint cracking (first crack through the central region of the joint).
- Beam bar yielding.
- Initiation of joint spalling (first flaking of concrete in joint region).
- Extensive joint spalling (exposure of center column bar in joint region).

The sequence in which they occurred differed, depending on the specimen properties. Center Joint Cracking and Beam Bar Yielding are self-explanatory. Initiation of Spalling and Extreme Spalling are less obvious states. Examples are shown in figures 5a and b.

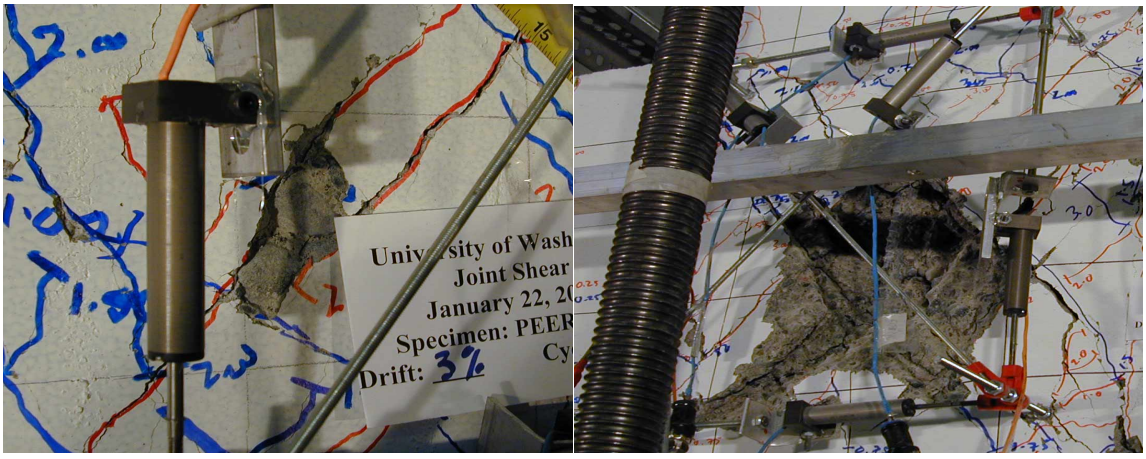

Figure 5 Initial Spalling (left) and Extensive Spalling (right).

Joint damage incurs repair costs, so it is of interest to relate the damage to some engineering parameter, such as drift or strain, so that it can be predicted from the results of a structural analysis. Damage was found to correlate best with joint strain. While it is not surprising that a local measure of deformation provides the best indictor of damage, it also emphasizes the need to include joint deformations in the analytical model. The damage cannot reliably be determined from a global parameter, such as drift, that would the only choice if the joint shear deformations were not available. Furthermore, the prediction of damage is likely to be most reliable if the joint model reflects the degradation with cycling.

SIMULATION OF JOINT STRESS-STRAIN RESPONSE

A constitutive model was developed to simulate the response of the experimental specimens. The model has the ability to capture the degradation effects in the joint stiffness and strength as well as increase in pinching that result from cycling. The following provides a brief description of the model development and calibration. The model is currently being implemented in the OPENSees structural analysis programming environment. A full description of the model development, operation, and implementation is provided in Anderson (2003).

Model Operation and Parameters

The proposed constitutive model was developed specifically to account for the important joint shear stress-strain curve characteristics demonstrated by the experimental results. Most importantly, the branch curves are controlled by relatively sophisticated rules to ensure that they reproduce correctly the wide range of observed behaviors. The key components of the model, illustrated in Figure 6, are:

- A tri-linear backbone curve, representing monotonic response
- Pre-yield and post-yield branch curves, to simulate cyclic deformation demands
- Functions to simulate degradation in strength and stiffness
- Pinched portions of the branch curves which degrade to represent the closing of increasingly wide cracks.

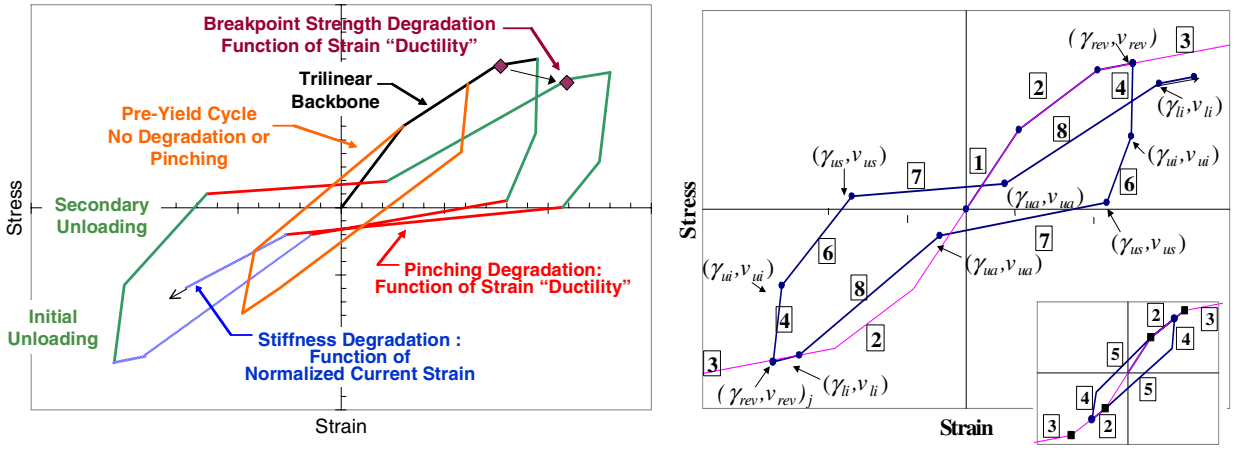

Figure 6: Characteristics of and Rules for Joint Shear Stress- Strain Constitutive Model

The backbone response is modeled using a tri-linear curve. For convenience, the breakpoints marking changes in stiffness are referred to as the 'cracking' and 'yield' points. However, they do not necessarily correspond to cracking of the joint core or yielding of the beam reinforcement.

The branch curves simulate the unloading and reloading responses, and their nonlinearity and degradation depend on the joint shear strain demand. The unloading or reloading portions of the branch curves are also tri-linear; the three segments are referred to as initial unloading, secondary unloading, and asymptotic unloading (Figure 6).
There are three categories of the joint response: pre-cracking, pre-yield, and post-yield response. The degree of inelastic action depends on the portion of the response curve in which the current strain lies. The response prior to cracking is modeled as elastic. The measured response indicates that cycling at strain levels below the threshold strain does not induce degradation. As such, in the model the pre-yield cycles result in inelastic loops that do not pinch or degrade (in the model the threshold strain is designated as the yield strain). Post-yield cycles induce pinching, stiffness and strength degradation.

In the three regions of the model, stress is obtained from strain using a series of hysteresis rules that are functions of input parameters and internal variables. The input parameters are constants supplied by the user and include stress and stiffness values that define the backbone curve as well as certain ratios that control cyclic behavior. Internal variables are used within the hysteresis rules and degradation functions, and their values change as loading progresses. In the following discussion, model input parameters are shown in bold and internal parameters are shown in italics. The input parameter and internal variable nomenclature is based on a system of main variables and primary and secondary subscripts. Main variables describe the type of parameter or internal variable; subscripts indicate the portion of the backbone or branch curve to which the parameter or variable applies. Outer subscripts are placed outside of parentheses and refer to the cycle number or direction.

Table 2 Hysteresis Rules

Rule	Segment	Label	Stiffness/Stress	Limits	Unloading	If Exceeded:
1	Pre-crack	cr	$G_{cr} = v_{cr}/\gamma_{cr}$	$\gamma_j < \gamma_{cr} < \gamma_{max}$	Rule 1	Rule 2
2	Pre-yield	yl	$G_{yl} = \frac{v_{yl} - v_{cr}}{\gamma_{yl} - \gamma_{cr}}$	$\gamma_{cr} < \gamma_j < \gamma_{yl} \le \gamma_{max}$	Rule 4	Rule 3
3	Post-yield	py	$G_{py} = r_{G.py} * G_{sec,yl}$	$\gamma_{yl} < \gamma_j$	Rule 4	N/A
4	Initial Unloading	ui	$G_{ui} = r_{G.ui} * G_{sec,yl}$ $v_{ui} = r_{v,ui} * v_{rev,i}$			
	Pre-yield			$\gamma_{ui} < \gamma_j < \gamma_{rev} < \gamma_{yl}$	Rule 4	Rule 5
	Post-yield			$\gamma_{yl} < \gamma_{max}$ $\gamma_{ui} < \gamma_j < \gamma_{rev}$	Rule 4	Rule 6
5	Secondary Unloading Pre-yield	us	$G_{us} = \frac{v_{ui} - v_{cr}}{\gamma_{ui} - \gamma_{cr}}$	$(\gamma_{yl})_{opp} < \gamma_j < \gamma_{ui} \le \gamma_{yl}$	Rule 4	Rule 2
6	Secondary Unloading Post-yield	us	$G_{us} = r_{G.us} * (G_{sec})_j$	$\gamma_{yl} < \gamma_{max}$ $\gamma_{us} < \gamma_j < \gamma_{ui}$	Rule 4	Rule 7
7	Asymptotic Unloading	ua	$G_{ua} = r_{G.ua} * G_{sec,yl}$	$\gamma_{yl} < \gamma_{max}$ $\gamma_{ua} < \gamma_j < \gamma_{us}$	Rule 4	Rule 8
8	Initial Loading Post-yield	li	$G_{li} = (G_{sec})_j = f(\alpha_{G,sec})$	$\gamma_{yl} < \gamma_{max}$ $\frac{\alpha_{v,yl} * v_{yl}}{(G_{sec})_j} < \gamma_j < \gamma_{ua}$	Rule 4	Rule 3

The monotonic backbone curve and the branch curves of the cyclic joint shear stress-strain response are defined by eight rules, as illustrated in Figure 6 and defined in Table 2. Three rules are used to define the backbone curve, two rules are needed for pre-yield branch curves, and an additional three rules are used to describe post-yield cycles. The stiffness rules are summarized in Table 2. The following provides a general description of the model components including model input and internal parameters and

associated main variables and subscripts. Recommended values for input parameters are provided in a later section.

Backbone Curve

A tri-linear backbone curve is used to model the monotonic response and envelope of the shear stress-strain response. The backbone curve is defined by two pairs of stress and stiffness input parameters ($\mathbf{v_{cr}}$, $\mathbf{G_{cr}}$ and $\mathbf{v_{yl}}$, $\mathbf{G_{sec,yl}}$). Rules 1-3 are described in Table 2. The variables $\mathbf{v_{cr}}$ and $\mathbf{G_{cr}}$ are respectively the stress and secant stiffness to the cracking breakpoint. Similarly, $\mathbf{v_{yl}}$ and $\mathbf{G_{sec,yl}}$ are the stress at yield and the secant stiffness from the origin to the yield point. This pair of variables defines the yield breakpoint. The yield strain, γ_{yl} is calculated as $\gamma_{yl} = \mathbf{v_{yl}} / \mathbf{G_{sec,yl}}$); strains larger than this induce degradation and pinching in the constitutive model. The input parameter $\mathbf{r_{G,py}}$ is a stiffness ratio (constant value) and is a multiplier on the yield secant stiffness $\mathbf{G_{sec,y}}$ to calculate the post-yield stiffness, $G_{py,}$ as:

$$G_{py} = \mathbf{r_{G,py}} * \mathbf{G_{sec,yl}} \qquad (1)$$

Pre-Yield Branch Curves

The branch curves are categorized as either pre-yield or post-yield, which determines the degree of degradation. Pre-yield branch curves consist of initial unloading and secondary unloading segments which are defined respectively by Rules 4 and 5 of Table 2. The initial unloading segment of the branch curve is the portion immediately following a reversal point (Segment 4 in Figure 6). The stiffness of the initial segment is designated as G_{ui} for an unloading segment. This stiffness is the product of an input stiffness ratio $\mathbf{r_{G,ui}}$ (recommended value of 20) and the yield secant stiffness $\mathbf{G_{sec,yl,}}$ which results in an expression similar to that provided by Eq. 1. The stress at the breakpoint between the initial and secondary unloading segments is designated v_{ui}. This stress is the product of the input stress ratio $\mathbf{r_{v,ui}}$ (recommended value of 0.65) and the stress at the reversal point of the cycle $v_{rev,j}$. The secondary pre-yield unloading stiffness, G_{us}, is the slope of the line connecting the end of the initial unloading segment at v_{ui} to the cracking point in the opposite quadrant (γ_{cr}, $\mathbf{v_{cr}}$) (see Rule 5 in Table 2).

Post-Yield Branch Curves

Post-yield branch curves are defined using rules for initial unloading, secondary unloading, asymptotic unloading (or pinching) and the initial reloading portion of the branch curve. The post-yield initial unloading segment is also defined using Rule 4. The secondary unloading stiffness, G_{us}, is a ratio of the yield secant stiffness, $\mathbf{G_{sec,yl,}}$ and a constant, $\mathbf{r_{G,us,}}$ as given by Rule 6 (Eq. 2). Observations indicate that this ratio increases with an increase in the joint shear stress demand. The recommended expression is given by Eq. 2:

$$G_{us} = \mathbf{r_{G,py}} * \mathbf{G_{sec,y\,l}}; \quad \mathbf{r_{G,py} = 0.2(v_j/(A_j\sqrt{f'_c})) + 0.59 \leq 3.5} \qquad (2)$$

One of the primary differences between the pre- and post-yield branch curves is the use of degradation parameters to reduce the strength and stiffness. Figure 7 shows the measured response of Specimens CD30-1450 and PEER-2250. Figure 7a illustrates the secant stiffness (from the origin) of the ascending curves and shows that the stiffness degrades significantly with increases in the strain demand. Figure 7b shows the breakpoint (location of abrupt change in stiffness) of the ascending curves. Again, significant stress degradation occurs at large strain values. As a result, the proposed degradation relationships are functions of normalized strain demands (as indicated in Figure 6). Relative to other cyclic models, they are simpler to track in that they do not depend on counting cycles or tracking the dissipated energy.

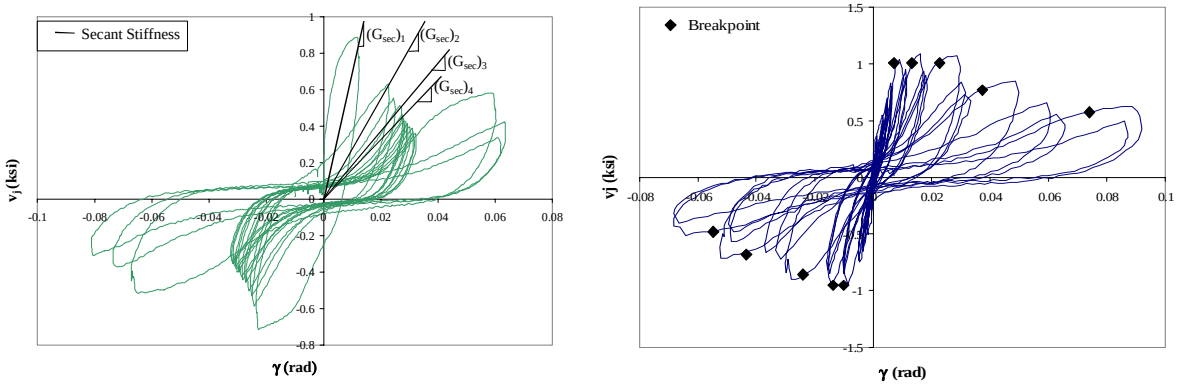

Figure 7 Influence of Strain Demand on (a) Stiffness and (b) Breakpoint Stress of Ascending Branch

Mathematical expressions were developed to model these two sources of degradation. Figure 6 illustrates both. The stiffness degrades only if the strain demand exceeds the current maximum strain reversal. Therefore, degradation in the secant stiffness of the ascending branch, $G_{j+1,sec}$ (for the j+1 cycle) is a nonlinear function of the strain demand for cycle j relative to the maximum reversal strain. If the strain limits are exceeded, the secant stiffness is calculated as:

$$\mathbf{G_{sec,j+1} = \alpha_{G,sec,j} * G_{sec,j}} \qquad (3)$$

For larger strain ratios, the multiplier, $\alpha_{G,sec}$, decreases. In addition, the stiffness degrades due to cycling in the opposite direction. This additional degradation is accounted for using a second multiplier (see Anderson 2002).

Degradation in the breakpoint stress occurred for strain demands that were large relative to the yield strain. Because the strain is normalized to the "yield" strain, this strain ratio is referred to as the strain ductility for convenience. Again, the multiplier on the breakpoint stress degrades with an increase in the strain ductility and with cycling in the opposite direction. Relations for each multiplier have been developed for the test specimens and are provided in Anderson (2002).

The experimental results indicate that pinching in the hysteresis curves becomes more severe with strain demands that exceed the yield strain. In the model, this response is represented analytically by a pair of degrading, pinching asymptotes. Each asymptote is defined by a number pair consisting of a stress intercept, $v_{ua,o}$, and secant stiffness values, G_{ua}. The pair of asymptote values is calculated using Equation 4, which degrades the stress and stiffness relative to the backbone yield values. The values of $r_{v,ua}$ and $r_{G,ua}$ are using degradation relations which are a function of the strain ductility values. The functions relating $r_{v,ua}$ and $r_{G,ua}$ to the strain ductility are tri-linear and decrease in value with an increase in the strain ductility. Calibrated functions are available in Anderson (2002), although the model is general and the functions may be defined by user input parameters. The breakpoint marking the initiation of pinching, v_{us} in Figure 6b, is the intersection of the secondary unloading leg of the branch curve and the unloading asymptote.

$$\mathbf{G_{ua} = r_{G,ua} * G_{yl}}$$
$$\mathbf{v_{ua} = r_{v,ua} * r_{yl}} \qquad (4)$$

The stiffness of the ascending branch of the curve that follows the pinching portion is referred to as initial loading and defined using Rule 8 in Table 2 (shown in Figure 6b) and Eq. 3. The breakpoint between the pinching asymptote and the initial loading segment, indicated by v_{ua} in Figure 6b, is the intersection of the unloading asymptote and the secant line defined by $G_{sec,j}$.

The previous discussion has summarized the operation of the constitutive model. Details and examples of model implementation are available in Anderson (2003).

Model Calibration and Validation

The experimental test data were used to calibrate the model parameters that determine the five model components. The calibration procedure was as follows: (1) Identify model parameters for each model component (as discussed in previous section). (2) Use measured trends to establish initial estimates of parameter relationship and values. (3) Minimize a local error measure to determine the best-fit expression and values for each model parameter. (4) Minimize a global error measure to refine the best-fit estimate. (5) Combine all best-fit expressions to develop a single recommended expression for each model parameter.

Individual best-fit expressions were developed for the data from each test series, since the model parameter may depend on the joint properties. For example, the monotonic response (or backbone response) curve depends on the joint shear stress demand but is independent of the displacement history. Therefore, all of the specimens within a test series (e.g., Test Series 1450) were used to develop a single best-fit calibration expression. The recommended expressions were derived using all of the best-fit expressions. Specific details on the calibration procedures, error measures, and the data-specific values may be found in the original reference (Anderson 2003).

The Walker-Alire experimental data were used to validate the constitutive model using the recommended expressions. The results indicate that the model is capable of approximating a range of joint shear stress demands and displacement histories, as shown in Figures 8 and 9. Figure 8 shows the measured and predicted responses of specimens PEER-1450 and PEER-2250, where PEER-1450 represents an average level of joint shear stress demand (and approximately equal to the ACI limit) and PEER-2250 represents a larger joint shear stress demand which may be found in existing construction (Mosier 2000). The results indicate that the model captures the cyclic responses of both specimens

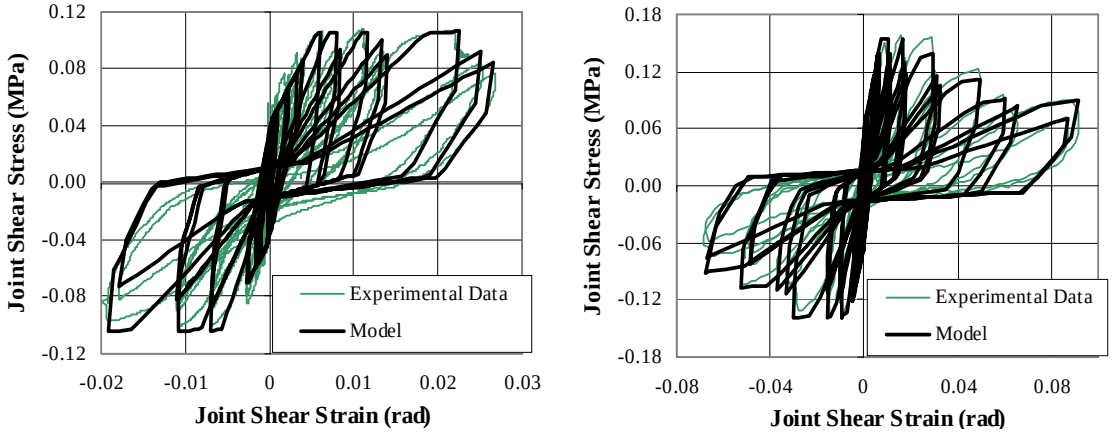

Figure 8 PEER-1450 and PEER-2250: Measured and Predicted Joint Shear Response

Previous research indicates that although other constitutive models may also effectively model standard deformation histories, few can adequately model unconventional histories (Anderson 2003). The proposed model is capable of modeling a wide range of shear strain histories, which represents a significant advancement. To illustrate this capability, the measured and predicted responses of specimens PADH-1450 and CD15-1450 are studied (Figure 9). The model is capable of predicting the slow degradation exhibited by CD15-1450 and the highly non-symmetric history of PADH-1450. The strength and stiffness of the final negative cycles of the PADH-1450 are over-predicted. However, these are cycles to 4% and 5% drift following a large 5% drift demand in the opposite direction and therefore modeling accuracy at

this large shear strain was sacrificed in order to permit better accuracy at the lower shear strain cycles (after the large pulse).

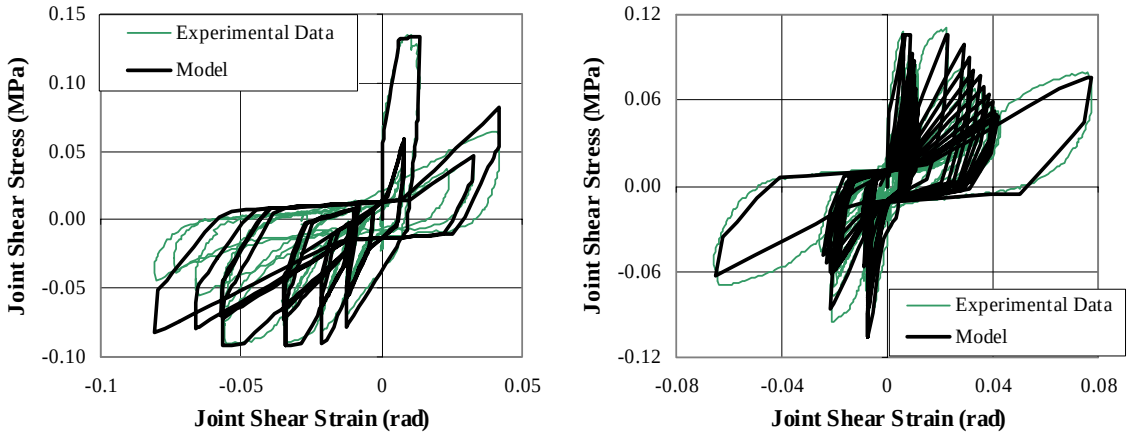

Figure 9 PADH-1450 and CD15-1450: Measured and Predicted Joint Shear Response

An independent experimental data set was used to further validate the model. For proper validation, the joint shear stress-strain data was needed and this is not always available. In addition, the specimen should model joints in non-ductile frame construction; few researchers have tested beam-column joints with little or no joint transverse reinforcement. Data from a specimen tested by Leon met the validation criteria (Leon 1990). The specimens had a peak joint shear stress demand of approximately $1.25\sqrt{f'_c}$ MPa ($15\sqrt{f'_c}$ (psi)) and a volumetric joint reinforcement ratio of approximately 0.6%. Figure 10 shows the measured and predicted responses of the specimen. The model predicts the cyclic response well, including degradation in the strength, stiffness, and pinching portion of the response.

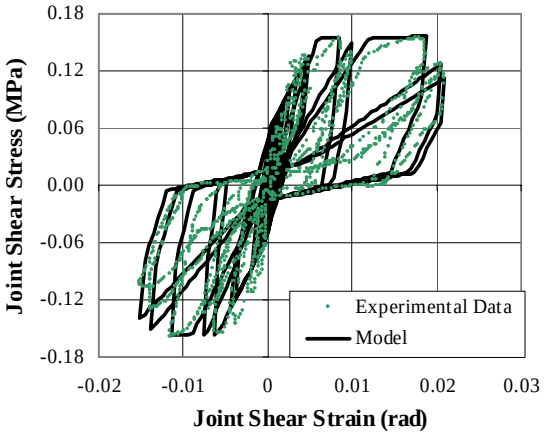

Figure 10 Measured and Predicted Response of Specimen BCJ2 (Leon 1990)

SUMMARY AND CONCLUSIONS

A test program was carried out to study the cyclic behavior of beam column joints in older reinforced concrete frames and designed to focus evaluating the joint shear behavior. The joints contained no transverse reinforcement, and the joint shear stress demand was varied by suitable selecting suitable beam bars. A primary study variable was the displacement history. Four different displacement histories were used which modeled the influence of asymmetric and constant-amplitude drift demands on the joint response. The experimental findings were used to evaluate the seismic performance of the specimen. Four aspects of joint performance were noted. First, the compressive strength of the joint must be sufficient to

carry the gravity load on the column and this condition was satisfied in every test. The second behavioral feature of interest showed that, for joints without transverse reinforcement the strength varies significantly with bar yielding and displacement history. The third and fourth critical features of joint behavior are the joint stiffness and damage accumulation, which both relate to the displacement history. During the course of the experiments, the joint stiffness dropped significantly as damage occurred which indicates that modeling the joints in a frame analysis as rigid is likely to lead to a significant underestimate of the lateral drift. The drift affects not only the damage to the non-structural components, but also the possibility of instability due to P-Δ effects. The primary damage states included cracking, yielding, joint spalling, and damage to the core concrete. Damage was found to correlate best with joint strain which also emphasizes the need to include joint deformations in the analytical model. Furthermore, a constitutive model for joint deformations should reflect the degradation with cycling.

The second phase of the research program was conducted to develop a constitutive model to simulate the degradation in the joint response and support performance evaluation of frames with joints without transverse reinforcement. To develop this model, measured joint shear strain data were used to establish general characteristics of the response in joints that represent pre-1970s construction. The proposed constitutive model was developed and calibrated using these observations. The model includes a backbone curve, to model the monotonic response, and unloading and reloading branch curves that consist of initial, secondary, and asymptotic (or pinching) segments. A series of expressions was developed for each component of the model. These expressions were calibrated using the experimental data and were simplified for general application of the model. Strength and stiffness degradation were explicitly included in the branch curves. The degradation expressions depend only on a characteristic of the previous strain history (e.g., the maximum reversal strain to date) rather than the entire strain history. In that respect, the model provides a unique method of accounting for cyclic degradation in that counting cycles or tracking energy is not required.

ACKNOWLEDGEMENTS

Funding for the experimental testing was provided by NSF under Award Number EEC-9701568 through the PEER center. The Department of Civil and Environmental Engineering at the University of Washington (UW) supported the graduate studies of Daniel Alire. The Valle Scholarship Program supported the graduate studies of Meredith Anderson. All sources of funding are gratefully acknowledged.

REFERENCES

ACI Committee 318 (2002). "Building Code Requirements for Structural Concrete (ACI 318-02) and Commentary (ACI 318R-02). ACI, Farmington Hills, MI.

Alire, D.A. (2002). "Seismic Evaluation of Existing Unconfined Reinforced Concrete Beam-Column Joints", MSCE Thesis, Dept. of Civil Engineering, University of Washington. 291 p.

Anderson, M.A. (2003). "Analytical Modeling of Existing Reinforced Concrete Beam-Column Joints", MSCE Thesis, Civil and Environmental Engineering, University of Washington. 308 p.

Durrani, A.J. and Wight, J.K.. (1985). "Behavior of Interior Beam-to-Column connection Under Earthquake-Type Loading", *ACI Jo.*, Title No. 82-30, ACI, Farmington Hills, MI, May-June. pp. 343-350.

Ehsani, M.R. and Wight, J.K.(1985). "Exterior R/C Beam-to-Column Connections Subjected to Earthquake-Type Loading", *ACI Jo.*, Title No. 82-43, ACI, Farmington Hills, MI, July-Aug. pp. 421-428.

Hanson, N., Connor, H. (1967) "Seismic Resistance of Reinforced Concrete Beam-Column Joints". *Proc. ASCE, Jo. Str. Div.*, 93(ST5), Oct., pp. 533-560.

Leon, R.T. (1990). “Shear Strength and Hysteretic Behavior of Interior Beam-Column Joints”, *ACI Str. Jo*., 87(1), Jan.-Feb. pp. 3-11

Meinheit, D.F. and Jirsa, J.O. (1981). “Shear Strength of RC Beam-Column Connections”. *Proc. ASCE, Jo. Str. Div.*, 107 (ST11), Nov. pp.

Raynor (2000). “Bond Assessment of Hybrid Fame Continuity Reinforcement”. MSCE Thesis, Dept. of Civil Engineering, University of Washington. 248 p.

“*Uniform Building Code*”. (1997). International Conference of Building Officials, Whittier, CA.

Walker, S.G. (2001). “Seismic Performance of Existing Reinforced Concrete Beam-Column Joints”. MSCE Thesis, Dept. of Civil Engineering, University of Washington. 308 p.